Journal of Controlled Release 239 (2016) 242–248

Contents lists available at ScienceDirect

Journal of Controlled Release

journal homepage: www.elsevier.com/locate/jconrel

Diffusion of water-soluble sorptive drugs in HEMA/MAA hydrogels

D.E. Liu [a,1], T.J. Dursch [a,1], N.O. Taylor [a], S.Y. Chan [a], D.T. Bregante [a], C.J. Radke [a,b,*]

[a] Chemical and Biomolecular Engineering Department, University of California, Berkeley, CA 94720, United States
[b] Vision Science Group, University of California, Berkeley, CA 94720, United States

ARTICLE INFO

Article history:
Received 27 April 2016
Received in revised form 21 July 2016
Accepted 22 August 2016
Available online 24 August 2016

Keywords:
Hydrogel
Drug
Adsorption
Diffusion
Controlled release
Polyelectrolyte

ABSTRACT

We measure and, for the first time, theoretically predict four prototypical aqueous-drug diffusion coefficients in five soft-contact-lens material hydrogels where solute-specific adsorption is pronounced. Two-photon fluorescence confocal microscopy and UV/Vis-absorption spectrophotometry assess transient solute concentration profiles and concentration histories, respectively. Diffusion coefficients are obtained for acetazolamide, riboflavin, sodium fluorescein, and theophylline in 2-hydroxyethyl methacrylate/methacrylic acid (HEMA/MAA) copolymer hydrogels as functions of composition, equilibrium water content (30–90%), and aqueous pH (2 and 7.4). At pH 2, MAA chains are nonionic, whereas at pH 7.4, MAA chains are anionic ($pK_a \approx 5.2$). All studied prototypical drugs specifically interact with HEMA and nonionic MAA (at pH 2) moieties. Conversely, none of the prototypical drugs adsorb specifically to anionic MAA (at pH 7.4) chains. As expected, diffusivities of adsorbing solutes are significantly diminished by specific interactions with hydrogel strands. Despite similar solute size, relative diffusion coefficients in the hydrogels span several orders of magnitude because of varying degrees of solute interactions with hydrogel-polymer chains. To provide a theoretical framework for the new diffusion data, we apply an effective-medium model extended for solute-specific interactions with hydrogel copolymer strands. Sorptive-diffusion kinetics is successfully described by local equilibrium and Henry's law. All necessary parameters are determined independently. Predicted diffusivities are in good agreement with experiment.

1. Introduction

Hydrogels are cross-linked polymeric networks that readily imbibe water and typically swell without dissolving [1–7]. The ability of hydrogels to uptake aqueous solutes and later release them in a controlled manner has led to their extensive use in drug delivery [1,4–6,8–15], tissue engineering [16–18], bioseparations [19,20], and biosensing [21–24]. For example, hydrogels have been recently introduced as soft contact lenses (SCLs) capable of detecting tear-film components and administering drugs and bioactive agents to the eye, allowing for early disease diagnosis and treatment [25,26]. Because solute and hydrogel properties (e.g., hydrophilicity, charge, and chemistry) vary significantly with application, solute release rates are highly system dependent. Accordingly, designing optimal solute-hydrogel combinations for controlled and targeted solute delivery remains a challenge.

Diffusion of aqueous solutes occurs primarily through the water-filled meshes of the hydrogel-polymer network [2,7,11,14,27–36]. Aqueous-solute diffusivities in hydrogels, D, are diminished relative to those in bulk solution, D_o, by nonspecific interaction with the hydrogel-polymer chains including steric obstruction and hydrodynamic resistance [2,7,11,14,27–36]. In many cases, aqueous-solute diffusivities are further diminished by specific complexation of solutes to hydrogel-polymer chains that arises when specific solute-hydrogel binding overcomes competing interactions with water [1–4,7,9,10,12,14,29,37–39]. Aqueous solutes may adsorb reversibly or irreversibly to the interior hydrogel network, hindering solute release rates by orders of magnitude. Consequently, solute-specific interactions (i.e., those other than electrostatic and finite size) with the hydrogel-polymer network often dictate the efficacy of hydrogels in applications requiring controlled and targeted release.

Because of the wide variety of applications, significant effort has been expended toward obtaining aqueous-solute diffusivities both experimentally [2,10–12,14,27–36,38–41] and theoretically [2,11,27–36,38,42–44]. Most published experimental work, however, focuses on diffusion of nonspecific-interacting aqueous solutes in high water-content hydrogels (i.e., >90%) [2,11,12,14,27–36,38,40,44]. As a result, theoretical models typically exploit dilute hydrogel-polymer fractions and consider almost exclusively hydrodynamic drag, available free-volume, and/or steric obstruction by hydrogel-polymer chains. Solute-specific interaction is often exhibited by polymers, polymeric surfactants, and proteins in SCL-material hydrogels and by ionic/nonionic drugs and vitamins in drug-delivery hydrogels [1,2,4,7,10,12,14,37–39,41]. To date, however, relatively little attention has been given to aqueous-solute

* Corresponding author at: Chemical and Biomolecular Engineering Department, University of California, 101E Gilman, Berkeley, CA 94720-1462, United States.
E-mail address: radke@berkeley.edu (C.J. Radke).
[1] Authors contributed equally.

http://dx.doi.org/10.1016/j.jconrel.2016.08.025
0168-3659/

diffusion in hydrogels where solute/polymer-chain interactions are significant.

We report experimental and theoretically predicted diffusion coefficients of four prototypical water-soluble drugs in hydrogels where solute-specific binding is pronounced [1]. The hydrogels studied are representative of SCL materials and are copolymers of 2-hydroxyethyl methacrylate (HEMA) and methacrylic acid (MAA). To vary the extent of solute adsorption, hydrogel copolymer composition was varied in HEMA:MAA weight ratios of 100:0, 99:1, 90:10, 70:30, and 0:100. All hydrogels are referred to by their corresponding wt% MAA, where wt% MAA and wt% HEMA sum to 100. Two-photon laser-scanning confocal microscopy and UV/Vis-absorption spectrophotometry with back extraction measure transient solute concentration profiles and concentration histories, respectively. Diffusion coefficients are obtained for theophylline, acetazolamide, sodium fluorescein, and riboflavin in five SCL-material hydrogels as a function of pH (2 and 7.4). We quantitatively predict prototypical drug diffusion coefficients by Large-Pore-Effective-Medium theory extended for specific-solute adsorption to each hydrogel copolymer type (HEMA or MAA) and assuming local equilibrium. All parameters are determined independently. In all cases, predicted solute diffusivities are in good agreement with experiment.

2. Materials and methods

2.1. Hydrogel synthesis and equilibrium water contents

Detailed hydrogel-synthesis and water-content-measurements are provided in Dursch et al. [1]. Here, we briefly summarize. HEMA/MAA hydrogels were synthesized by simultaneous copolymerization and cross-linking of monomers in aqueous solution with EGDMA as the cross-linking agent [1–3]. Aqueous synthesis mixtures consisted of varying HEMA:MAA ratios (100:0, 99:1, 90:10, 70:30, and 0:100), 0.25 wt% EGDMA, and 30 wt% DI water. All percentages are of total monomer. Following free-radical polymerization, hydrogels were swollen or deswollen in excess aqueous buffered saline solutions of varying pH, but with equal ionic strength: phosphate-buffered saline solution (PBS; pH 7.4; 0.017 M Na_2HPO_4, 0.003 M NaH_2PO_4, 0.15 M NaCl, [1–3]) and dilute HCl (pH 2; 0.02 M HCl, 0.15 M NaCl). Solutions were changed daily for a minimum of 3 d to ensure equilibrium with the surrounding solution. All measurements were performed at ambient temperature (22–25 °C).

2.2. Solute loading

Equilibrium swollen hydrogels were soaked for a minimum of 2 d in solute solutions with a solution-to-hydrogel volume ratio of 250. Initial loading concentrations for sodium fluorescein were 1×10^{-5} M and 1×10^{-7} M in PBS and HCl solutions, respectively. Initial loading concentrations for riboflavin, theophylline, acetazolamide were 1×10^{-5} M, 6×10^{-3} M and 2×10^{-3} M, respectively, in both PBS and HCl. At these dilute concentrations, solute uptake had no measurable effect on hydrogel water content. To ensure equilibrium solute uptake, solute loading time was increased until no change was observed in solute partition coefficients measured according to Dursch et al. [1].

2.3. Two-photon fluorescence confocal microscopy

Sodium fluorescein and riboflavin diffusion coefficients in the hydrogels were obtained by solute desorption measurements with two-photon laser-scanning confocal microscopy as described in Liu et al. [2]. Transient concentration profiles were measured using a Carl Zeiss (Jena, Germany) 510 LSM META NLO AxioImager Confocal Microscope equipped with a Spectra-Physics (Santa Clara, CA) MaiTai HP DeepSee Laser set at 780 nm. In short, equilibrium solute-loaded hydrogel flats (6 mm × 6 mm and 100–800 μm thick) were each placed in a large bath of pertinent solute-free aqueous solution (PBS or HCl) under magnetic stirring at 400 rpm. At selected times, a gel flat was removed from solution, placed on a microscope slide, and covered with a cover slip to prevent evaporation. Scanning was performed in the center at 3-μm intervals through the entire gel thickness and resulting micrographs were converted into intensity profiles. At the dilute concentrations employed, fluorescence intensity is linearly proportional to dye concentration [2]. Fig. 1 displays typical fluorescence intensity as a function of position for sodium fluorescein desorbing from a 10 wt% MAA hydrogel at various release times. The distance scale denotes top to bottom of the hydrogel. Intensity profiles are not perfectly symmetric due to signal attenuation [2]. As discussed in Appendix A, overall solute-hydrogel diffusion coefficients are obtained by fitting Fick's second law in Eq. A1 to fluorescent-solute intensity profiles by least-squares error minimization [2]. Dashed lines in Fig. 1 illustrate typical fits. Note in Fig. 1 that in PBS all sodium fluorescein eventually leaches from the gel indicating reversible release.

2.4. Back extraction with UV/Vis-absorption spectrophotometry

Theophylline and acetazolamide diffusion coefficients in the hydrogels were determined through desorption with back extraction. Back-extraction solution concentration histories were measured with UV/Vis-absorption spectrophotometry by a procedure adapted from Dursch et al. [1]. An Ocean Optics spectrophotometer (Model ADC-1000, Dunedin, FL) equipped with a deuterium UV/Vis DH-2000 light source was employed for aqueous-solution absorbance measurement. 6 mm × 6 mm × ~400 μm gel slabs were solute loaded in excess solution. After equilibration, the hydrogels were removed from their loading solution, lightly blotted on both sides, and immediately placed in a large volume of pertinent solute-free aqueous solution (PBS or HCl) under magnetic stirring at 400 rpm. Typical release-solution-to-hydrogel volume ratios ranged from 20 to 2000 and were set for accurate measurement of release-solution concentration. Transient back-extraction solution concentrations were measured by periodically removing 2 mL of solvent and measuring previously calibrated solution absorbance at 220–250 nm in a 4-mm wide UV quartz cuvette (path length 10 mm). Measurements were performed in triplicate to account for minor fluctuations in detected absorbance. All 2-mL samples were returned to the release solution to maintain constant solution volume. Fig. 2 displays typical back-extraction-solution concentrations as a function of time for theophylline desorbing from a 10 wt% MAA hydrogel in PBS. Concentration transients are for desorption. We close mass balance in the back-extraction experiments confirming reversible interactions of solute with the gel matrix.

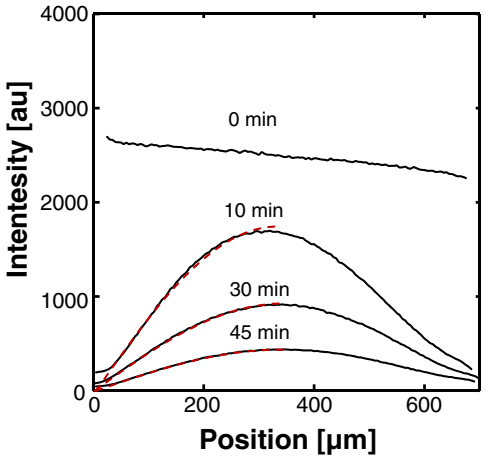

Fig. 1. Transient intensity profiles of sodium fluorescein desorption from a 10 wt% MAA hydrogel immersed in PBS. Solid and dashed lines represent measured profiles and least-square fits to Fick's second law, respectively.

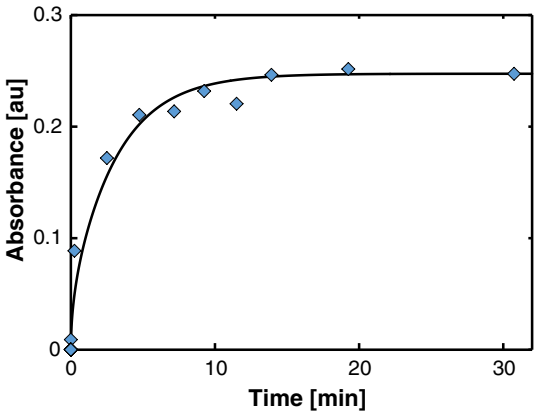

Fig. 2. Release solution absorbance as a function of time for theophylline desorption from a 10 wt% MAA hydrogel immersed in PBS. The solid line represents a least-square fit to Fick's second law.

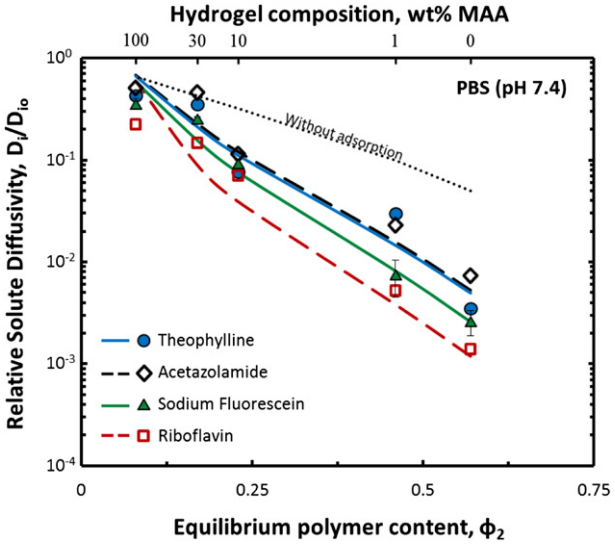

Fig. 3. Relative solute diffusion coefficients, D_i/D_{io}, as functions of polymer volume fraction, φ_2, for theophylline (closed circles), acetazolamide (open diamonds), sodium fluorescein (closed triangles), and riboflavin (open squares), in HEMA/MAA hydrogels equilibrated in PBS (pH 7.4). Typical error bars are shown. Solid and dashed lines are drawn according to theory with adsorption (i.e., Eq. 4 with Henry's adsorption constant, K_{ij}, specified by EFPT). Solid and dashed lines correspond to filled and open symbols, respectively. The dotted line is drawn for acetazolamide according to theory without adsorption (i.e., Eq. 4 with $K_{ij}=0$ for all j).

To ensure that our results are independent of the experimental technique employed, select riboflavin and sodium fluorescein diffusion coefficients at each aqueous pH were obtained by both UV/Vis-absorption spectrophotometry and two-photon confocal microscopy. Consistency was confirmed as both methods yielded nearly identical solute diffusion coefficients (i.e., within experimental error).

3. Experimental results

To assess the extent of solute-specific binding to hydrogel-polymer chains, equilibrium partition coefficients of dilute solute i, k_i (defined as the ratio of average solute concentration per unit volume of gel to the bulk aqueous-solute concentration), were obtained following Dursch et al. [1]. Table 1 displays k_i for theophylline, acetazolamide, sodium fluorescein, and riboflavin in HEMA/MAA hydrogels equilibrated in aqueous PBS and HCl. Also shown are hydrogel equilibrium water volume fractions, φ_1. At pH 7.4, sodium fluorescein ($pK_a = 4.5, 6.5$) is dianionic and acetazolamide ($pK_a = 7.2$) is partially anionic, whereas all other solutes are neutral. As discussed elsewhere [1], $k_i > \varphi_1$ for all solutes in 0 wt% MAA hydrogels (i.e., 100 wt% HEMA) reveals specific adsorption to HEMA copolymer chains, most significant for riboflavin. Conversely, similar k_i (~0.7) for nearly all solutes in 100 wt% MAA hydrogels is due to similar solute Stoke's radii (0.37–0.62 nm [1,45]) and nonspecific-interaction with ionized MAA [1]. Table 1 also displays k_i in HEMA/MAA hydrogels equilibrated in HCl (pH 2) where all solutes and hydrogels are uncharged. At this lower pH, all solutes exhibit $k_i > \varphi_1$ in all hydrogels, most significant by uncharged sodium fluorescein. Accordingly, measured k_i values clearly demonstrate the presence of specific solute/polymer-chain interactions in the HEMA/MAA hydrogels.

Aqueous-solute diffusion coefficients were obtained for all solute-hydrogel systems reported in Table 1. Fig. 3 graphs measured solute diffusion coefficients relative to their bulk aqueous values, D_i/D_{io}, as a function of equilibrium polymer volume fraction, φ_2, in the HEMA/MAA hydrogels equilibrated in PBS (pH 7.4). For reference, all bulk-aqueous drug diffusion coefficients, D_{io}, are provided in Table 2. Lines in Fig. 3 are drawn according to theory discussed below (i.e., Eq. 4). As expected, D_i/D_{io} for all solutes decreases with rising φ_2 (i.e., increasing HEMA copolymer fraction), corresponding to smaller available meshes for solute diffusion, increased hydrodynamic drag, and increased tortuosity. In MAA homopolymer hydrogels (i.e., $\varphi_2 = 0.08$), where copolymer-chains are anionic and nonspecifically-interacting, relative diffusion coefficients are similar for all solutes. However, despite all solutes being of similar size, relative diffusion coefficients vary by orders of magnitude in HEMA-containing hydrogels of the same composition (and, accordingly, identical φ_2). Notably, riboflavin, which displays the strongest interaction with HEMA-copolymer strands (i.e., the largest k_i in Table 1 for 0% MAA hydrogels), also exhibits the smallest relative diffusion coefficient for all HEMA-containing hydrogels. Clearly, diffusion rates are significantly reduced by solute adsorption to HEMA-copolymer strands.

At pH 2, all solutes are neutral and specifically adsorb to both HEMA and nonionic MAA moieties. Fig. 4 again displays relative solute-hydrogel diffusion coefficients for the four prototypical drugs, but now as a function of the MAA-copolymer content for hydrogels equilibrated in HCl (pH 2). Here, D_i/D_{io} is plotted against wt% MAA rather than against φ_2 because addition of MAA copolymer at pH 2 results in a non-monotonic change in φ_2 (see Table 1). Similar to Fig. 3, lines in Fig. 4 correspond to relative diffusion coefficients predicted *a priori* from theory discussed below. D_i/D_{io} initially declines with addition of uncharged

Table 1
Hydrogel water contents and solute partition coefficients with varying HEMA:MAA weight ratios in aqueous PBS/HCl[a].

Hydrogel composition (HEMA:MAA)	Water content[b] ϕ_1	Theophyline[b]	Acetazolamide[b]	Sodium fluorescein[b]	Riboflavin[c]
100:0	0.43/0.40	2.8/2.8	2.5/4.4	2.4/103.2	5.4/5.4
99:1	0.54/0.39	2.4/2.9	2.1/4.3	1.7/136.5	5.3/4.6
90:10	0.77/0.29	1.8/3.2	1.3/3.8	0.7/111.8	2.5/5.8
70:30	0.83/0.31	1.2/3.5	1.0/3.2	0.2/118.2	1.4/5.2
0:100	0.92/0.71	0.7/5.8	0.6/1.8	0.1/133.0	0.7/5.4

[a] Table entries separated by a diagonal represent partition coefficients measured in PBS (pH 7.4) or HCl (pH 2).
[b] From Dursch et al. [1].
[c] Measured by two-photon fluorescence confocal microscopy with 780-nm excitation according to Dursch et al. [1].

Table 2
Bulk-aqueous solute diffusion coefficients and hydrodynamic radii.

Solute	$D_{io}\times10^6$ [cm^2/s]	Hydrodynamic radius [nm]
Theophylline[a]	6.7	0.37
Acetazolamide[a]	6.1	0.41
Riboflavin[b]	4.2	0.58
Sodium fluorescein[a]	4.0	0.62

[a] From Dursch et al. [1].
[b] Hydrodrodynamic radius from Shin et al. [45]. D_{io} is calculated using the Stokes-Einstein equation at 25 °C.

MAA (0% to 10%) and a consequent rise in φ_2 (0.60 to 0.71). However, with further addition of MAA (10% to 100%), D_i/D_{io} rises for all solutes due to the sharp decline in φ_2 (0.71 to 0.29). Again, despite similar solute size, relative diffusion coefficients vary by orders of magnitude in HEMA-containing hydrogels of identical water content. This observation is again attributed to reduced diffusion rates arising from specific interactions with HEMA-copolymer chains. Here, however, relative diffusion coefficients also vary by orders of magnitude in 100% MAA hydrogels, suggesting solute-specific interactions with electrically neutral MAA-copolymer strands. Notably, acetazolamide exhibits both the greatest D_i/D_{io} value and the smallest k_i (1.8 in Table 1) of the five solutes in 100% MAA hydrogels at pH 2. In comparison to those of acetazolamide, the lower D_i/D_{io} values for theophylline and riboflavin in 100 wt% MAA hydrogels are complemented by larger k_i values (5.8 and 5.4 in Table 1, respectively). A greater reduction of D_i/D_{io} is exhibited by solutes of stronger specific interactions with MAA-copolymer. For all hydrogels, the smallest relative diffusion coefficients are exhibited by uncharged sodium fluorescein that displays the highest adsorption to both HEMA- and neutral MAA-copolymer chains. Evidently, solute-specific interactions with both HEMA- and neutral MAA-copolymer chains account for the reduced diffusion rates seen at pH 2.

4. Theory and comparison

Available models for aqueous solute diffusion in hydrogels almost exclusively consider diffusion through the water-filled meshes of the nonspecifically-interacting hydrogel network [11,27–35,38,42–44]. However, Figs. 3 and 4 demonstrate that specific-solute complexation

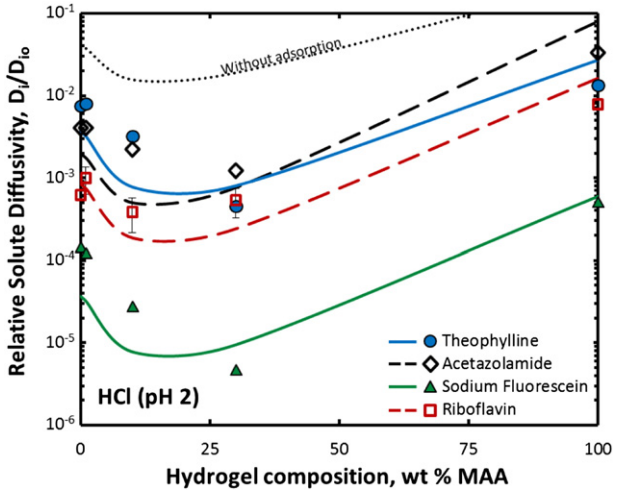

Fig. 4. Relative solute diffusion coefficients, D_i/D_{io}, as functions of MAA copolymer content for theophylline (closed circles), acetazolamide (open diamonds), sodium fluorescein (closed triangles), and riboflavin (open squares) in HEMA/MAA hydrogels equilibrated in HCl (pH 2). Typical error bars are shown. Solid and dashed lines are drawn according to theory with adsorption (i.e., Eq. 4 with Henry's adsorption constant, K_{ij}, specified by EFPT). Solid and dashed lines correspond to filled and open symbols, respectively. The dotted line is drawn for acetazolamide according to theory without adsorption (Eq. 4 with $K_{ij}=0$ for all j).

with hydrogel copolymer strands can drastically reduce diffusion rates. We desire a procedure to predict solute diffusion in hydrogels where specific solute adsorption is significant. For this task, it proves useful to discriminate between solutes diffusing in the water filled voids and solute adsorbed onto each hydrogel-copolymer component or,

$$C_i = \sum_j \varphi_{2,j} n_{ij} + \varphi_1 C_i^L \tag{1}$$

where C_i is the average solute concentration in the hydrogel per unit gel volume, $\varphi_{2,j}$ is the volume fraction of polymer component j, φ_1 is the water volume fraction, and n_{ij} and C_i^L are the concentrations of solute i specifically adsorbed to hydrogel polymer strands (mol/polymer volume) and diffusing through the water-filled meshes (mol/liquid volume), respectively. Upon extending Fick's second law in Eq. A1 with this classification, we write that

$$\sum_j \varphi_{2,j}\frac{\partial n_{ij}}{\partial t} + \varphi_1\frac{\partial C_i^L}{\partial t} = \varphi_1 D_i^L \frac{\partial^2 C_i^L}{\partial x^2} \tag{2}$$

where D_i^L is the solute diffusion coefficient through the water-filled meshes of the hydrogel network. Here, diffusion along the polymer strands is assumed negligible. To describe the kinetics of solute adsorption to each hydrogel copolymer type (i.e., HEMA, anionic MAA, or nonionic MAA), we impose local equilibrium with Henry's adsorption [1], or $n_{ij}=K_{ij}C_i^L$, where K_{ij} is the Henry's adsorption constant of the diffusing solute i to polymer component j. Here subscript j denotes HEMA, anionic MAA (at pH 7.4), or nonionic MAA (at pH 2). Local equilibrium requires that: (1) solute adsorption is reversible (i.e., solutes desorb from hydrogel polymer strands), and (2) rates of solute adsorption and desorption are faster than the rate of diffusion through the water-filled meshes of the polymer network [2]. Our confocal-microscopy and back-extraction experiments confirm reversible desorption of the four studied solutes from the five studied hydrogels. Strong solute-hydrogel-polymer interactions lead to greater irreversibility with rates of solute adsorption much larger than those of desorption [2]. Accordingly, local equilibrium applies when specific-solute adsorption is modest, as quantified by modest Henry adsorption constants.

Upon substitution of Henry's law for each copolymer component (i.e., $n_{ij}=K_{ij}C_i^L$) into Eq. 2, an overall effective diffusion coefficient arises, or

$$D_i = \frac{D_i^L}{1+\sum_j K_{ij}\varphi_{2j}/\varphi_1} \tag{3}$$

Notably, the overall diffusion coefficient is that predicted for nonspecifically interacting solutes, D_i^L, divided by a retardation factor accounting for specific adsorption. The retardation factor in the denominator of Eq. 3 is equivalent to the adsorption enhancement factor in Enhancement Factor Partitioning theory (EFPT) [1]. Without specific solute

Table 3
Henry's adsorption constant (dimensionless).

Solute	K_{iHEMA}[a]	K_{iMAA-}[b]	K_{iMAA}[c]
Theophylline[d]	7.5/7.5	0	21
Acetazolamide[d]	6.5/13	0	5
Riboflavin[e]	21/21	0	26
Sodium fluorescein[d]	8.5/~455	0	~730

[a] Table entries separated by a diagonal represent k_i measured in PBS (pH 7.4) or HCl (pH 2).
[b] In PBS (pH 7.4).
[c] In HCl (pH 2).
[d] From Dursch et al. [1].
[e] Measured by two-photon confocal microscopy with 780 nm excitation according to Dursch et al. [1].

adsorption to the polymer chains (i.e., $K_{ij} = 0$ for all j), Eq. 3 reduces to the diffusion coefficient for nonspecifically interacting solutes.

Values for K_{ij} were calculated for all j by applying EFPT to the equilibrium partitioning data in Table 1 [1]. Table 3 displays Henry's adsorption constants calculated from EFPT for HEMA, anionic MAA, and nonionic MAA. Notably, nearly all specific solute-copolymer interactions are weak to moderate with $K_{ij} < 30$ supporting our imposition of local equilibrium. Stronger specific complexation is only exhibited by sodium fluorescein at pH 2 with HEMA and with nonionic MAA.

The nonspecific-interacting solute diffusivity, D_i^L in Eq. 3, is calculated by Large-Pore-Effective-Medium (LPEM) theory [2]. LPEM theory accounts for hydrodynamic drag, steric obstruction, and the accessible meshes available to diffusing solutes. Solutes are permitted only to access meshes larger than their size and solely experience hydrodynamic drag and steric obstruction within those accessible meshes [2]. Accordingly, terms for both hydrodynamic drag and steric obstruction are calculated over the distribution of mesh sizes available for solute transport. A complete description of LPEM is available elsewhere [2]. Upon normalizing Eq. 3 by the solute diffusion coefficient in bulk solution, D_{io}, and by expressing D_i^L/D_{io} as the product of hydrodynamic and steric resistance factors from LPEM we, establish that.

$$\frac{D_i}{D_{io}} = \frac{F_i S_i}{1 + \sum_j K_{ij}\varphi_{2j}/\varphi_1} \tag{4}$$

where F_i and S_i are hydrodynamic and steric resistance factors, respectively. F_i and S_i are calculated *a priori* using Large-Pore Effective Medium (LPEM) theory with an average polymer fiber radius of, $a_f = 2$ nm, and a hydrodynamic tortuosity of, $\tau_H = 4.7$, both determined through independent measurement [2,3]. With F_i and S_i given by LPEM and K_{ij} specified by EFPT, Eq. 4 permits *a priori* calculation of relative solute-hydrogel diffusion coefficients for all prototypical drugs as a function of hydrogel composition and aqueous pH.

Lines in Fig. 3 compare predicted and measured D_i/D_{io} of the prototypical drugs as a function of φ_2 in aqueous PBS. A dotted line in Fig. 3 is drawn according to Eq. 4 without specific solute-polymer-chain interactions (i.e., $K_{ij} = 0$ for all j) for acetazolamide. Predictions without adsorption for the remaining prototypical drugs are similar due to similar solute size [2], and are not shown for clarity. Predicted D_i/D_{io} values without adsorption decline with rising φ_2 because of increased hydrodynamic drag and steric obstruction. However, quantitative agreement is lacking. Without accounting for specific adsorption, theory consistently over predicts measured D_i/D_{io} by orders of magnitude.

As discussed above, all studied prototypical drugs specifically adsorb to HEMA chains reducing release rates in HEMA-containing hydrogels. Solid and dashed lines in Fig. 3 are drawn according to Eq. 4 with specific adsorption (i.e., with K_{ij} in Table 3). Predicted D_i/D_{io} now decline more drastically due to solute-specific adsorption to HEMA copolymer chains, in addition to the increased nonspecific interactions (i.e., F and S in Eq. 4). With increasing HEMA copolymer content, however, lines diverge between the various solutes due to varying degrees of specific interaction with HEMA copolymer. Because all Henry's adsorption constants are measured independently [1], no adjustable parameters appear in the proposed theory. Nevertheless, agreement between theory and experiment is excellent.

Similar to Fig. 3, lines in Fig. 4 compare predicted and measured D_i/D_{io} for the aqueous drugs as a function of MAA copolymer content, now in dilute aqueous HCl. Again a dotted line is drawn for acetazolamide neglecting specific solute-polymer-chain interactions (i.e., $K_{ij} = 0$ for all j). Predictions without adsorption (not shown) are similar for all studied prototypical drugs again due to similar solute size [2]. Agreement between theory without adsorption and experiment is poor. Without specific interactions, theory again over predicts measured D_i/D_{io} values.

In HCl (pH 2), all of the water-soluble drugs specifically interact with both HEMA and uncharged MAA chains, dramatically reducing diffusion rates in the hydrogels studied. Solid and dashed lines in Fig. 4 are drawn according to theory with specific adsorption (i.e., with K_{ij} specified by EFPT). Good agreement between theory with adsorption and experiment is also observed at pH 2. Consequently, specific adsorption is vital to quantify release rates from hydrogels when solute-specific binding is pronounced.

Discrepancies between theory and experiment in HCl (pH 2) may be explained by the low φ_1 of the studied hydrogels. Available theories predicting D_i/D_{io} from nonspecific interactions were derived for high-water-content hydrogels [2,28–31,34,44]. Extrapolation of those theories to lower φ_1 systems incurs increasing error in predicting hydrodynamic drag, steric obstruction, and the distribution of mesh sizes available for solute transport [2]. Additionally, with lower φ_1, fewer water-filled voids are accessible for solute diffusion and more polymer strands are available for solute-specific complexation. Consequently, accurate description of solute-specific interactions with hydrogel polymer chains is critical at lower φ_1.

At pH 2, sodium fluorescein exhibits strong specific complexation with HEMA and MAA copolymer chains with k_i two orders of magnitude greater than φ_1 of HEMA/MAA hydrogels. Complete release from the lowest φ_1 hydrogels (30% and 10% MAA) is not observed even after one month of release, indicating substantial irreversibility [1]. Nevertheless, Eq. 4 provides a good first approximation to estimate solute release rates. In spite of no adjustable parameters, near quantitative prediction is achieved for all prototypical drugs in all hydrogels at both aqueous pH values.

The importance of specific adsorption in predicting solute release rates from hydrogels is readily apparent in a parity plot. Fig. 5 displays D_i/D_{io} predicted by theory versus those measured by experiment on log-log scales for the prototypical drugs in the HEMA/MAA hydrogels at both aqueous pH 2 and pH 7.4. A linear unity-slope straight line is included for reference. Closed and open symbols denote predictions from Eq. 4 with adsorption (i.e., with finite K_{ij} in Table 3) and without adsorption (i.e., with $K_{ij} = 0$ for all j), respectively. Predictions without specific interactions consistently overestimate the data by orders of magnitude, most significantly for those solutes with the strongest interactions with the hydrogel polymer chains (i.e., those with the largest k_i in Table 1). In contrast, predictions including specific interactions display excellent agreement with experiment. Successful agreement of theory with experiment also validates the model assumption of local sorption equilibrium. For the solutes and hydrogels examined in this work, adsorption and desorption kinetic rates are faster than diffusion rates: there is no

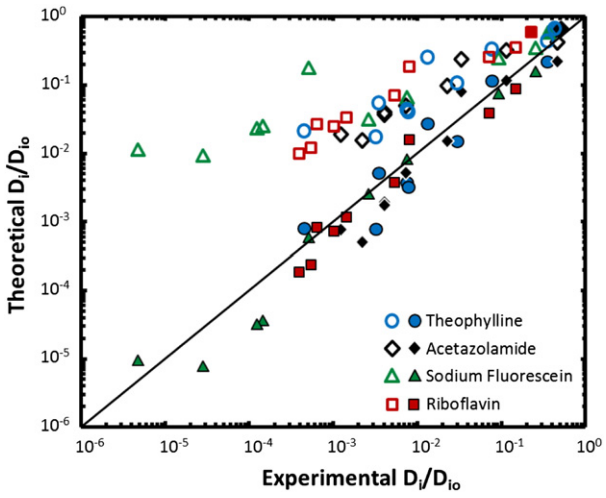

Fig. 5. Parity plot of theoretical and experimental relative solute diffusion coefficients, D_i/D_{io} for acetazolamide (diamonds), sodium fluorescein (triangles), theophylline (circles), and riboflavin (squares), in HEMA/MAA hydrogels. Closed and open symbols denote predictions from Eq. 4 with adsorption (i.e., with Henry's adsorption constant, K_{ij}, specified by EFPT) and without adsorption (i.e., $K_{ij} = 0$ for all j), respectively.

need to incorporate sorption kinetics. We note that the over prediction from neglect of specific adsorption is not an artifact of LPEM theory. Non-specific interactions were also calculated *a priori* using other physical-based models [28,30,31,43,44]; identical trends were observed. Solute-specific interactions with the hydrogel-polymer chains are critical to ascertain rates of prototypical drug transient release from hydrogels.

5. Conclusions

We obtained molecular diffusion coefficients of four prototypical drugs in soft-contact lens material hydrogels of varying copolymer composition and aqueous pH using two-photon fluorescence confocal microscopy and UV/Vis-absorption spectrophotometry. All prototypical drugs studied exhibited specific adsorption to nonionic MAA and HEMA moieties. Solute release rates were significantly diminished by specific interactions, most apparent at pH 2 where solute adsorption is strong. Measured relative diffusivities span several orders of magnitude, which is attributed to varying degrees of solute-specific interactions with hydrogel-polymer strands. By invoking local equilibrium and Henry-law adsorption, diffusion coefficients are quantitatively predicted using an LPEM model extended for solute-specific interactions with the hydrogel-polymer chains. Predicted diffusion coefficients are in good agreement with experiment using no adjustable parameters. Our new framework provides *a priori* quantitative prediction of specifically interacting solute uptake and release rates in hydrogels.

Acknowledgements

The authors thank the CRL Molecular Imaging Center and NIH grant number 3R01EY015514-01S1 for use of the fluorescence confocal microscope. The authors also thank Xiaoyi Li and Ryan Sawadichai for performing several of the UV/Vis-absorption spectrophotometry measurements.

Appendix A

To describe the rate of solute release from hydrogels, we utilize Fick's second law.

$$\frac{\partial C_i}{\partial t} = D_i \frac{\partial^2 C_i}{\partial x^2} \quad -L<x<L \tag{A1}$$

where C_i is the solute concentration of dilute solute i in the hydrogel per unit gel volume, D_i is the overall solute diffusion coefficient through the gel, and x is the spatial coordinate for a hydrogel thickness of 2 L with x = 0 at the center of the hydrogel flat. Since the hydrogels are thin relative to their 6-mm y- and z-coordinate length scales, solute transport is approximately one dimensional in x. Initially, $C_i(t,0) = C_{io}$, where C_{io} is the final solute concentration in a hydrogel equilibrated with aqueous-solute loading solution (i.e., $C_{io} = k_i C_{iS}$ where k_i is the solute partition coefficient in the hydrogel and C_{iS} is the bulk aqueous-solute concentration in the loading solution). The perfect-sink boundary condition is applied to Eq. A1, or $C_i(L,t) = 0$, since we assume the concentration at the edge of the gel is in equilibrium with the surrounding aqueous release solution, and the latter is in excess and devoid of solute. Additionally, $\partial C_i(0,t)/\partial x = 0$, since theoretical profiles are symmetric about the center of the gel. Integration of Eq. A1 with the boundary and initial conditions specified gives

$$\frac{C_i(t,x)}{C_{io}} = \sum_{n=0}^{\infty} A_n(t,x) \tag{A2}$$

where $A_n(t,x) = 2\frac{(-1)^n}{\lambda_n} exp[-{\lambda_n}^2 D_i t/L^2] \cos[\lambda_n x/L]$ and $\lambda_n = (2n+1)\pi/2$ [2]. To obtain overall solute-hydrogel diffusion coefficients by two-photon confocal microscopy, Eq. A2 is fit to fluorescent-solute intensity profiles by least-squares error minimization as described in Liu et al. [2].

For back extraction with UV/Vis-absorption spectrophotometry, we desire an expression for the solute concentration in the back-extraction solution. Mass balance dictates the accumulation of solute in the surrounding back-extraction solution is equal to the amount of solute released from the gel, or

$$V_S \frac{dC_{iS}}{dt} = \frac{2V_g}{L}\left[-D_i \frac{\partial C_i}{\partial x}\right]_{x=L} \tag{A3}$$

where C_{iS} is the concentration of dilute solute i in the back-extraction solution, V_S and V_g are the volumes of the back-extraction solution and of the hydrogel slab, respectively and $[-D_i \partial C_i/\partial x]_{x=L}$ is the flux of solute desorbing from a face of the hydrogel slab. Substituting Eq. A1 into Eq. A3 and integrating over time yields

$$\frac{C_{iS}(t)}{C_{iS}(t=\infty)} = \sum_{n=0}^{\infty} \frac{1-\exp\left[-\left(\frac{(2n+1)\pi}{2}\right)^2 \frac{D_i t}{L^2}\right]}{(2n+1)^2} \tag{A4}$$

where $C_{iS}(t=\infty)$ is the equilibrium back-extraction aqueous-solute concentration. To obtain overall solute-hydrogel diffusion coefficients by back extraction, Eq. A4 is fit to back-extraction solute concentration histories by least-squares error minimization.

References

[1] T.J. Dursch, N.O. Taylor, D.E. Liu, R.Y. Wu, J.M. Prausnitz, C.J. Radke, Water-soluble drug partitioning and adsorption in HEMA/MAA hydrogels, Biomaterials 35 (2014) 620–629.
[2] D.E. Liu, C. Kotsmar, F. Nguyen, T. Sells, N.O. Taylor, J.M. Prausnitz, C.J. Radke, Macromolecule sorption and diffusion in HEMA/MAA hydrogels, Ind. Eng. Chem. Res. 52 (2013) 18109–18120.
[3] C. Kotsmar, T. Sells, N. Taylor, D.E. Liu, J.M. Prausnitz, C.J. Radke, Aqueous solute partitioning and mesh size in HEMA/MAA hydrogels, Macromolecules 45 (2012) 9177–9187.
[4] D.E. Liu, T.J. Dursch, Y. Oh, D.T. Bregante, S.Y. Chan, C.J. Radke, Equilibrium water and solute uptake in silicone hydrogels, Acta Biomater. 18 (2015) 112–117.
[5] N.A. Peppas, P. Bures, W. Leobandung, H. Ichikawa, Hydrogels in pharmaceutical formulations, Eur. J. Pharm. Biopharm. 50 (2000) 27–46.
[6] N.A. Peppas, Hydrogels and drug delivery, Curr. Opin. Colloid Interf. Sci. 2 (1997) 531–537.
[7] T.J. Dursch, D.E. Liu, Y. Oh, C.J. Radke, Fluorescent solute-partitioning characterization of layered soft contact lenses, Acta Biomater. 15 (2015) 48–54.
[8] P. Gupta, K. Vermani, S. Garg, Hydrogels: from controlled release to pH-responsive drug delivery, Drug Discov. Today 7 (2002) 569–579.
[9] C.-C. Peng, M.T. Burke, A. Chauhan, Transport of topical anesthetics in vitamin E loaded silicone hydrogel contact lenses, Langmuir 28 (2011) 1478–1487.
[10] J. Kim, A. Chauhan, Dexamethasone transport and ocular delivery from poly (hydroxyethyl methacrylate) gels, Int. J. Pharm. 353 (2008) 205–222.
[11] J.L. Stringer, N.A. Peppas, Diffusion of small molecular weight drugs in radiation-crosslinked poly (ethylene oxide) hydrogels, J. Control. Release 42 (1996) 195–202.
[12] R. Bettini, P. Colombo, N.A. Peppas, Solubility effects on drug transport through pH-sensitive, swelling-controlled release systems: transport of theophylline and metoclopramide monohydrochloride, J. Control. Release 37 (1995) 105–111.
[13] Y. Kapoor, J.C. Thomas, G. Tan, V.T. John, A. Chauhan, Surfactant-laden soft contact lenses for extended delivery of ophthalmic drugs, Biomaterials 30 (2009) 867–878.
[14] M.T. Am Ende, N.A. Peppas, Transport of ionizable drugs and proteins in crosslinked poly (acrylic acid) and poly (acrylic acid-co-2-hydroxyethyl methacrylate) hydrogels. II. Diffusion and release studies, J. Control. Release 48 (1997) 47–56.
[15] D.M. Eckmann, R.J. Composto, A. Tsourkas, V.R. Muzykantov, Nanogel carrier design for targeted drug delivery, J. Mater. Chem. B 2 (2014) 8085–8097.
[16] K.Y. Lee, D.J. Mooney, Hydrogels for tissue engineering, Chem. Rev. 101 (2001) 1869–1880.
[17] J.L. Drury, D.J. Mooney, Hydrogels for tissue engineering: scaffold design variables and applications, Biomaterials 24 (2003) 4337–4351.
[18] A. Khademhosseini, R. Langer, Microengineered hydrogels for tissue engineering, Biomaterials 28 (2007) 5087–5092.
[19] J.J. Kim, K. Park, Smart hydrogels for bioseparation, Bioseparation 7 (1998) 177–184.
[20] I. Roy, M.N. Gupta, Smart polymeric materials: emerging biochemical applications, Chem. Biol. 10 (2003) 1161–1171.
[21] S. Brahim, D. Narinesingh, A. Guiseppi-Elie, Bio-smart hydrogels: co-joined molecular recognition and signal transduction in biosensor fabrication and drug delivery, Biosens. Bioelectron. 17 (2002) 973–981.
[22] G. Lin, S. Chang, H. Hao, P. Tathireddy, M. Orthner, J. Magda, F. Solzbacher, Osmotic swelling pressure response of smart hydrogels suitable for chronically implantable glucose sensors, Sensor. Actuat. B-Chem. 144 (2010) 332–336.

[23] G. Lin, S. Chang, C.-H. Kuo, J. Magda, F. Solzbacher, Free swelling and confined smart hydrogels for applications in chemomechanical sensors for physiological monitoring, Sensor. Actuat. B-Chem. 136 (2009) 186–195.
[24] J. Liu, Oligonucleotide-functionalized hydrogels as stimuli responsive materials and biosensors, Soft Matter 7 (2011) 6757–6767.
[25] H. Yao, A.J. Shum, M. Cowan, I. Lähdesmäki, B.A. Parviz, A contact lens with embedded sensor for monitoring tear glucose level, Biosens. Bioelectron. 26 (2011) 3290–3296.
[26] R. Badugu, J.R. Lakowicz, C.D. Geddes, A glucose sensing contact lens: a non-invasive technique for continuous physiological glucose monitoring, J. Fluoresc. 13 (2003) 371–374.
[27] B. Amsden, Solute diffusion in hydrogels: an examination of the retardation effect, Polym. Gels Networks 6 (1998) 13–43.
[28] R.J. Phillips, A hydrodynamic model for hindered diffusion of proteins and micelles in hydrogels, Biophys. J. 79 (2000) 3350–3353.
[29] L. Johansson, C. Elvingson, U. Skantze, J.E. Löfroth, Diffusion and interaction in gels and solutions, in: C. Helm, M. Lösche, H. Möhwald (Eds.), Trends in Colloid and Interface Science VI, Springer, New York 1992, pp. 25–29.
[30] A.G. Ogston, B.N. Preston, J.D. Wells, On the transport of compact particles through solutions of chain-polymers, Proc. R. Soc. Lond. A 333 (1973) 297–316.
[31] E.M. Johnson, D.A. Berk, R.K. Jain, W.M. Deen, Hindered diffusion in agarose gels: test of effective medium model, Biophys. J. 70 (1996) 1017–1023.
[32] J. Tong, J.L. Anderson, Partitioning and diffusion of proteins and linear polymers in polyacrylamide gels, Biophys. J. 70 (1996) 1505–1513.
[33] N.A. Peppas, C.T. Reinhart, Solute diffusion in swollen membranes: Part I. A new theory, J. Membr. Sci. 15 (1983) 275–287.
[34] B. Amsden, Solute diffusion within hydrogels: mechanisms and models, Macromolecules 31 (1998) 8382–8395.
[35] R.J. Phillips, W.M. Deen, J.F. Brady, Hindered transport in fibrous membranes and gels: effect of solute size and fiber configuration, J. Colloid Interface Sci. 139 (1990) 363–373.
[36] J.C. Bosma, J.A. Wesselingh, Partitioning and diffusion of large molecules in fibrous structures, J. Chromatogr. B Biomed. Sci. Appl. 743 (2000) 169–180.
[37] J. Wu, A.P. Sassi, H.W. Blanch, J.M. Prausnitz, Partitioning of proteins between an aqueous solution and a weakly-ionizable polyelectrolyte hydrogel, Polymer 37 (1996) 4803–4808.
[38] E.W. Merrill, K.A. Dennison, C. Sung, Partitioning and diffusion of solutes in hydrogels of poly(ethylene oxide), Biomaterials 14 (1993) 1117–1126.
[39] L.C. Bengani, J. Leclerc, A. Chauhan, Lysozyme transport in p-HEMA hydrogel contact lenses, J. Colloid Interface Sci. 386 (2012) 441–450.
[40] S.M. Russell, E.B. Belcher, G. Carta, Protein partitioning and transport in supported cationic acrylamide-based hydrogels, AIChE J 49 (2003) 1168–1177.
[41] F. Rossi, F. Castiglione, M. Ferro, P. Marchini, E. Mauri, M. Moioli, A. Mele, M. Masi, Drug–polymer interactions in hydrogel-based drug-delivery systems: an experimental and theoretical study, ChemPhysChem 16 (2015) 2818–2825.
[42] N.A. Hadjiev, B.G. Amsden, An assessment of the ability of the obstruction-scaling model to estimate solute diffusion coefficients in hydrogels, J. Control. Release 199 (2015) 10–16.
[43] L. Johansson, C. Elvingson, J.E. Löfroth, Diffusion and interaction in gels and solutions. 3. Theoretical results on the obstruction effect, Macromolecules 24 (1991) 6024–6029.
[44] D.S. Clague, R.J. Phillips, Hindered diffusion of spherical macromolecules through dilute fibrous media, Phys. Fluids 8 (1996) 1720.
[45] H.S. Shin, S.Y. Kim, Y.M. Lee, K.H. Lee, S.J. Kim, C.E. Rogers, Permeation of solutes through interpenetrating polymer network hydrogels composed of poly(vinyl alcohol) and poly(acrylic acid), J. Appl. Polym. Sci. 69 (1998) 479–486.